

SOUND GENERATION BY RIGID CYLINDER INSERTED IN FLOW AS A NEW BENCHMARK PROBLEM FOR AIRFRAME NOISE

Victor Kopeiev, Nikolay Ostrikov, Mikhail Zaitsev*
Marc Terracol, Eric Manoha**

*TsAGI, Acoustic Division, Russia, Email: vkopiev@mx.iki.rssi.ru,

**ONERA, France, Email: marc.terracol@onera.fr

Key words: airframe noise, bluff body, turbulent wake, dipole and quadrupole sources, microphone array, azimuthal decomposition technique (ADT), large eddy simulation (LES).

Abstract Well-known situation when bluff body is streamlining by turbulent flow is considered. Recently obtained experimental results for cylinder and role of small quadrupole sources in the wake are discussed. They appear to be strongly connected with the dipole sources located on the cylinder. Interference leads to surprising picture of the resulting sound field detected in experiment: equivalent dipole sources are located in the wake zone far downstream from the cylinder (truncated cylinders). The understanding of the effect of dipole abnormal shift helps to elaborate the modified cylinder configurations which are considered. These configurations present attractive variant of airframe noise control where control realized by self-tuning of reflected signal leading to suppression of uncompensated dipoles. Careful 3D numerical simulation of dipole noise for the cylinders (round and truncated) using LES was carried out. Numerical calculation is validated by measurements under consideration. Numerical result is in agreement with the main conclusion that truncation of cylinder leads to noise suppression in wide frequency range. Therefore streamlining the cylinder could be considered as a new benchmark problem in airframe noise field. This problem demonstrates the measure of our success in describing of main peculiarities of novel experiments.

1. INTRODUCTION

With continued success in engine noise reduction, airframe noise has emerged as a potentially significant contributor to overall acoustic emissions, particularly at landing conditions. The dominant sources of airframe noise are known to be associated with unsteadiness of separated and/or vortex flow regions around the high-lift system (i.e., flaps and slats) and the aircraft undercarriage (i.e. landing gear). Due to the complexity of three-dimensional vortices that may contribute to flow unsteadiness and the importance of surface geometry in transformation of vortex motion into sound, airframe noise is an extremely complex and challenging problem ¹.

Investigations of the dipole type radiation when rigid body is inserted in turbulent flow have a many years history and are generally based on Lighthill-Curle approximation ^{2,3}. It was realized that the dipole sources are the result of non-stationary action of the body surface on the fluid ^{4,5,6}. From this point of view the dipoles are localized on the body surface and are the main source of sound in low frequency range. The other point of view on this phenomenon is based on replacing the boundary by the image source distribution (method of "image sources") ^{7,8,9,10}. In such an approach the

problem of calculation of dipole sources is usually restricted to simple body geometry (plane, sphere, cylinder etc.) and small Mach number. Approach, based on boundary Green function has some benefit because it keeps the direct connection between vorticity fluctuation and surface dipoles. It becomes more popular nowadays^{11,12} especially bearing in mind the noise control problem.

In the first part of the paper we briefly discuss the effect of dipole shift, firstly obtained and explained in^{13,14}. It was recognized that the dipole sources on cylinder and quadrupole sources in flow downstream the cylinder form the coherent interacting pair which changes the picture of total noise. The effective shift of dipole detects the dual role of small quadrupole sources in the low frequency range: (i) quadrupoles located closely to the cylindrical surface create the dipole sources in the cylinder (which radiate the main noise) and (ii) quadrupoles shift the equivalent dipole sources far downstream due to the interference.

This picture demonstrates two possible ways for separation flow noise control. The first (traditional) way provides the turbulence suppression in separation zone (quadrupole source intensity suppression). The second one provides suppression of reflected dipole due to surface (acoustic boundary condition) manipulation and does not provide for the turbulence intensity control. Therefore the first way is close to the flow control ideas but the second is the noise control way when we try to control the radiation mechanisms only without considerable changing the disturbances containing the main flow energy.

The understanding of the effect of dipole abnormal shift as self-tuning effect for reflected quadrupole helped to suggest in¹⁴ the modified cylinder configurations, which lead to considerable noise suppression (and force pulsation corresponding to the dipole moment of flow field as well). It was established that for the cylinder (nose leg or engine stator rack) with a plane rear surface the noise level in wide frequency band decreases by the value up to 5 dB over the whole range of observation angles. This not evident result was obtained in the series of experiments carried out in an anechoic chamber¹⁴.

We consider in the first part of this paper some new analytical results to understand more carefully the mechanism of noise suppression by truncated cylinder, using the conform mapping of truncated form to circular one. It appears that truncated surface could play twofold role: when the sources are located closely to the middle of truncated part it will act as a noise suppressor. If the sources are located closely to the sharp corner (curvature is much more) the noise is increased considerably and truncated part acts as an amplifier. One way is to measure turbulence characteristics by hot-wire, PIV, LDIS anemometer. We will not discuss the advantages or disadvantages of these methods here. Obviously the best way to recognize the turbulence structure and the structure of noise sources for exact 3D configuration would be numerical simulation of the problem. However to be sure of the accuracy of numerical results in turbulence simulation it is necessary to tune the numerical method using f.i. the acoustic measurement peculiarities (such as dipole shift, azimuthal structure of dipole noise etc.). Therefore the problem as a whole takes on special significance as a benchmark problem for the numerical method in airframe noise field and bluff body noise in particular.

In the second part of the paper, we focus on three-dimensional LES of the problem, using ONERA's in-house aeroacoustic solver, *sAbrina*^{28, 29, 30, 31}. The noise suppression by truncated configuration was confirmed in numerical simulation. It shows that this numerical method could be adequate to the problem as a whole and the total verification will be considered in the next paper.

2. MAIN APPROACH

Consider the problem of noise generation by a dipole source, using the cylinder streamline by a turbulent flow as an example. It is known^{2,3}, that Curle's equation in the case of fixed boundaries reduces to the following expression:

$$4\pi c_0^2 \rho = \frac{\partial^2}{\partial x_i \partial x_j} \int [T_{ij}] \frac{d^3 y}{|x-y|} - \frac{\partial}{\partial x_i} \oint \delta_{ij} p \frac{d s_j(y)}{|x-y|} \quad (1)$$

$$[T_{ij}] = T_{ij} \left(y, t - \frac{|x-y|}{c_0} \right), \quad T_{ij} = \rho v_i v_j + \delta_{ij} (p - c_0^2 \rho)$$

where ρ is the density, T_{ij} is Lighthill tensor, p is the pressure, v_i is the velocity, c_0 is the sound velocity, δ_{ij} is the Kronecker delta, the summation is assumed over the repeated indices. The first term in (1) corresponds to quadrupole radiation associated with turbulent fluctuations. The second term is connected with force fluctuations over a hard surface and corresponds to dipole radiation. At small Mach numbers and large wave lengths expression (1) is significantly simplified and takes the following form:

$$4\pi p = \frac{x_j x_k}{c_0^2 x} \frac{1}{x} \frac{\partial^2}{\partial t^2} \int [T_{jk}] d^3 y + \frac{x_j}{c_0 x} \cdot \frac{1}{x} \left[\frac{d F_j(t)}{dt} \right] \quad (2)$$

where square brackets mean a retarded time $t \rightarrow t - r/c_0$. Evaluating the value orders, one can easily find that dipole term P_d associated with fluctuations of the overall force $F_i(t)$ applied to the body radiates in terms of energy M^{-2} times more effectively, than quadrupole one P_q , associated with vortex fluctuations. Therefore it is generally accepted that the first term in (2) can be neglected in the cases of small Mach numbers ($M^2 \ll 1$) and long waves. However, even in these cases this term can be significant.

Actually, the dipole term in (2) is localized on the body surface. From this point of view the dipole appearance in the wake zone seems to be absolutely unfeasible. However, the shift of dipole into the region far downstream from the cylinder takes place in experiment. One possible explanation is as follows: the dipole sources on cylinder and quadrupole sources in flow downstream the cylinder (first and second terms in (2) form the coherent interacting pair which changes the picture of total noise. The effective shift of dipole detects the dual role of small quadrupole sources in the low frequency range: (i) quadrupoles located closely to the cylindrical surface create the dipole sources in the cylinder (which radiate the main noise) and (ii) quadrupoles shift the equivalent dipole sources far downstream due to the interference. So the first term neglect practically prevents from an understanding of the physical mechanism of dipole generation and makes impossible an explanation of new experimental facts.

3. ROUND CYLINDER

3.1 Experimental setup

Let the iron rod be inserted into a turbulent jet. As it is well known, the dipole noise is generated in this case. The jet issued at 100 m/s in velocity from a conical nozzle $D=4$ cm in diameter. The initial turbulence level in the exit nozzle plane was

$\varepsilon_0 = 0,2\%$. The cylinder of 1.2cm diameter (Figure 1) corresponded to the initial Reynolds number $Re \sim 8 \cdot 10^4$ introduced into a turbulent flow normally to the flow axis in the region to 5 calibers along the axis ($x=20$ cm) was used for dipole noise generation (Figure 2).



Figure 1. Circular cylinder

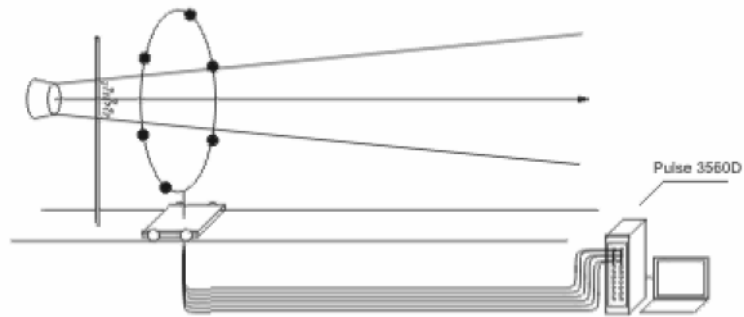


Figure 2. Scheme of experimental setup

The acoustic measurements were carried out in the far field with the use of 6 microphones (B&K, type 4135, Figure 2) located in the angles of a regular hexagon at the distance of 0,85m from the jet axis^{12,13}. The microphone signals were simultaneously supplied to 24-bit DAQ board NI 4472. The use of NI 4472 permitted obtaining simultaneously the power spectra of the reference signals themselves and of their linear combinations which are the components of the sound field expansion in Fourier transform in terms of the azimuthal angle.

3.2. Measurements of azimuthal components in the rod streamline noise

The zone of flow interaction with the rod is localized in a small volume. In principle, all the three dipoles components are possible: along the flow (drag dipole), normally to the jet and to the rod (lift dipole) and along the rod (viscous dipole). As the experiments show, the third dipole connected with viscous forces along the rod is negligibly small¹³.

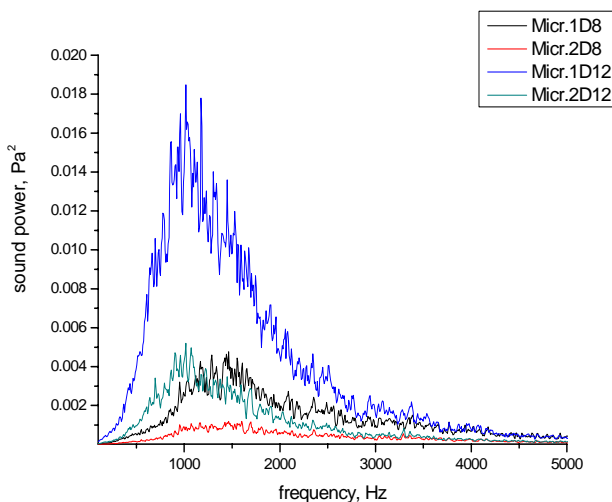


Figure 3. Spectra of two different array microphones (micr. 1 and 2, D=12cm) compared with truncated cylinder in the same microphone positions (micr. 1 and 2, L=8cm, Figure12).

The region of measurements is confined by the frequency ~ 3 kHz (Figure 3). To determine the directivity of the sound field produced by the turbulent source, we used the azimuthal decomposition method^{15,16,17,18,19}. The microphone array itself was shifted along the axis z , sweeping over the cylindrical surface in the far field covering up to 50 calibers along the axis. The rod coordinate corresponds to $x=20$ cm along the jet axis. For the vertical rod the radiation consists of two components: lift dipole (a_1) and drag dipole

(a_0). It means that viscous force play a minor role in the radiation for the experiment conditions. Note, that Figure4 presents the result which, at the first sight, defies common sense: the dipole directivity is shifted downstream by the value equal to $\sim 5-10$ cm, i.e. by the value equal to ~ 20 rod diameters. Since we know that in the downstream region there are only turbulent fluctuations (intensified by the separation zone), the advent of dipoles in this zone is impossible. The explanation of this interesting effect, suggested in ^{13,14} is discussed later.

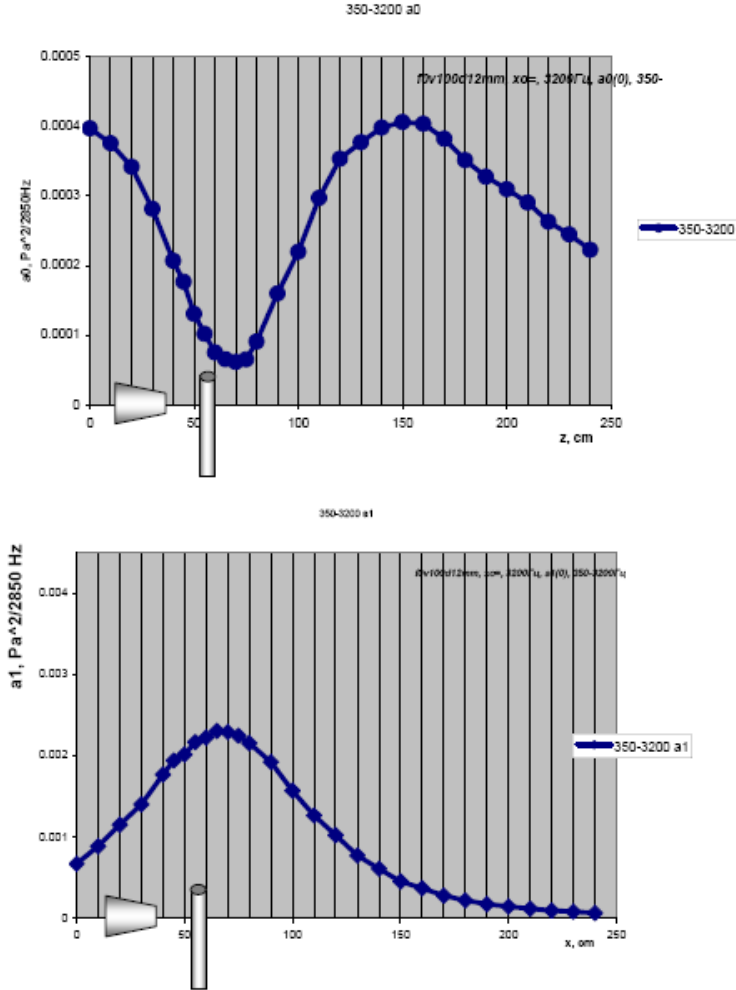


Figure 4. Two modes $a_0^2(x)$ ($n=0$) and $a_1^2(x)$ ($n=1$) in 350-3200Hz frequency band for cylinder $D=12\text{mm}$. The pictures demonstrate abnormal shift of dipole source (minimum for a_0 and maximum for a_1) far downstream the cylinder location.

3.3. Analysis of multipole shift near the curved surface and physical background of noise suppression mechanism.

Since the dipole term determined by the second term in (2) is localized deliberately in the rod region, the curve directivity shift along the jet axis can be associated only with the first term caused by turbulent fluctuations. We are limited our measurements by a long wave. In this case, as it is known, the region of radiation can be considered in an incompressible approximation. Let a vorticity distribution localized in the finite region with a characteristic dimension R and the size of a body be a . The unsteady movement of vortices is accompanied by sound wave radiation. At small

Mach numbers the flow can be characterized by different length scales: in the vorticity region (internal region) - by dimensions R and a , and in the far field (external region) where disturbances are small and are of wave structure - by the sound wave length scale λ . We consider the situation when wavelength λ considerably exceeds the characteristic dimensions R and a . The presence of two characteristic scales in different flow regions in the task of sound generation by vortices leads to the necessity of using the method of singular disturbances.

The investigation of sound generation by three-dimensional localized vortices in a weakly compressible fluid with the use of methods of singular disturbances was the object of a number of works starting from the first investigations^{20,21}. It was found that for the unbound fluid (fluid at rest on infinity without body) we could consider the inner region in incompressible approximation for resolving two approximations in the sound field in Mach number expansion - quadrupole and octupole. It seems believable that for the problem under consideration we could obtain two major terms in the sound field based on incompressible approximation but these terms are dipole and quadrupole.

Let only a dipole moment D_j be in the reference coordinate system and all the other source distributions be equal to zero. Consider this distribution in the coordinate system shifted by $-\delta_i$ relatively to the reference one (this corresponds to the dipole shifted by δ_i). It is easy to get²²:

$$\varphi = \frac{1}{r} \left[-\frac{x_i}{r^2} D_j + \frac{x_j x_k}{r^3} P_{jk} + \dots \right], \quad \text{where } P_{jk} = \delta_k D_j \quad (3)$$

Thus in the incompressible fluid, the dipole shifted from the origin of the coordinates with accuracy of small octupole is equivalent to the reference dipole and to the reference quadrupole in the origin of the coordinates.

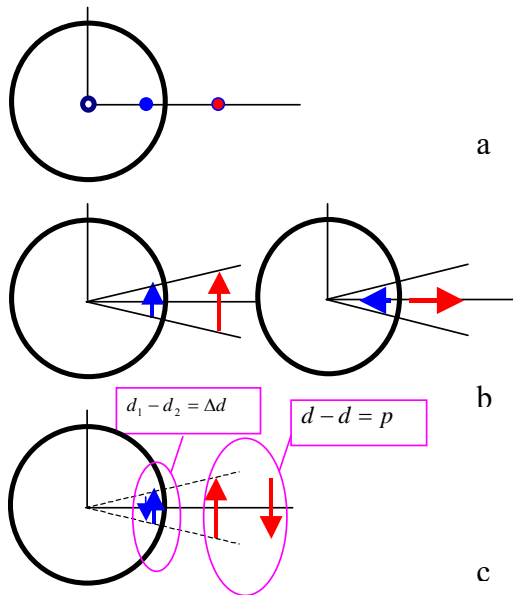


Figure 5. Scheme of point source location near hard cylinder in incompressible fluid. Red color – source, blue – image; q – monopole, d – dipole, p – quadrupole

Now turn our attention to the experimental results. The dipole obtained in the measurements, shifted to the origin of the coordinates means that the quadrupole term must be taken into account and for long acoustic waves we could trace the situation in some details.

Consider the incompressible problem when there is a point source of monopole type near the plane. If the source q and its reflection produces a pair on sources in the principal approximation with common intensity $2q$. If this source is a dipole, then in dependency of its orientation, two cases can be realized: dipole intensity doubling, or dipole moment reduction with quadrupole formation. The situation of doubling or reduction to octupole is also possible for a quadrupole.

Let a dipole be positioned near the cylinder (two sources q and $-q$ at points R and $R+l$). Similarly to the case with a plane, two situations are possible. In the case (a) reflected dipole will be extracted from the reference one, and in the case (b) they will be summarized (Figure 5b). However, the extraction will not be complete, as in the case with a half-plane. Really, for a dipole with moment $d = lq$ the induced dipole will have the same sources $\pm q$, but located at points a^2/R and $a^2/(R+l)$. Therefore the distance between the sources will be $(a^2/R^2)l$ and the overall intensity of both dipoles will be $(1 - a^2/R^2)ql$. Substituting this expression in (5), we obtain the long wave approximation for the radiated sound being in a complete agreement with the result which one could obtain using Howe reciprocal theorem method²³. This dipole intensity drops to zero only at $R \rightarrow a$. In the case (b) the dipole intensities are summarized and the overall intensity will be $(1 + a^2/R^2)ql$, and in the case $a \rightarrow R$ it is doubled as for the reflection in the plane.

Consider now a quadrupole near the cylinder (Figure 5c), consisting of two opposite dipoles with components $-P_{xy} = P_{yx} = ql^2 = p$. The absence of complete dipole reduction is of extreme importance, when the quadrupole reflection is considered. At reflection the dipole centres occur at conjugated points and the dipole which is reverently at point $R+l$ will have a less dipole moment in the case of reflection, than dipole R , since the source intensities are kept at reflection and the geometrical distances between the sources-images vary. The moment of the dipole, which is closer to the cylinder surface, will be $d_1 = ql(a/R)^2$ and the moment of the dipole which is more far from it, will be $d_2 = -ql(a/R)^2(1 - 2l/R)$. After summarizing, these dipoles do not compensate each other and the dipole of the following intensity appears:

$$\Delta d_y = \frac{2ql^2a^2}{R^3} = \frac{2pa^2}{R^3} \quad (4)$$

Thus, a quadrupole source with intensity p leads to occurrence of a reflected dipole with intensity $d = 2pa^2/R^3$, i.e. at $R \sim a$ of the same order in intensity. Since the dipole at $\lambda \gg a$ is a much more effective radiator, exactly it will dominate in the far field, i.e. a weak quadrupole source near a cylinder generates dipole noise many times exceeding it in intensity. Besides, the quadrupole source itself appears in a required phase to the created dipole and the summarized field according to (5) appears to be equivalent to that shifted (Figure6) along x at the distance

$$\delta = (a/2)(R/a)^3 \quad (5)$$

This shift will be more then 10 times larger than the diameter of the rod itself. A similar situation arises for p_{xx} quadrupole. In this case a dipole moment d_x appears and this dipole will be also shifted along axis x due to the quadrupole which generates it.

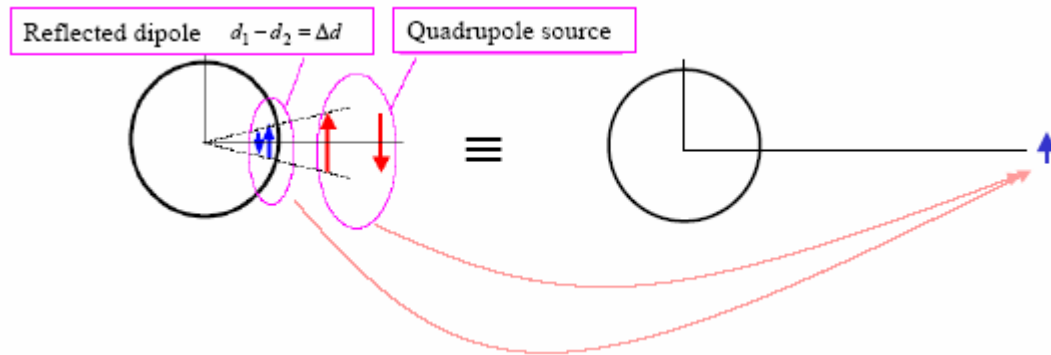


Figure 6. Scheme of dipole shift effect

As it was shown, this quadrupole source becomes much stronger close to the curve-lined hard surface due to appearance of the non-compensated dipole component, which arises as the result of quadrupole reflection from the hard body surface (Figure 7). When the curvature of the hard surface, from which the quadrupole source is reflected, decreases the dipole noise component reduces and disappears completely for the plane surface of reflection (Figure 8).

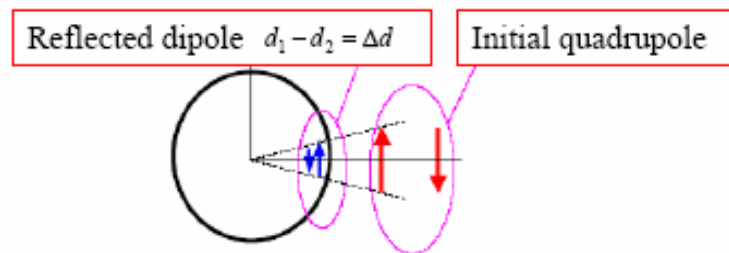


Figure 7. Scheme of the quadrupole noise source reflection from the curve-lined (cylindrical) hard surface.

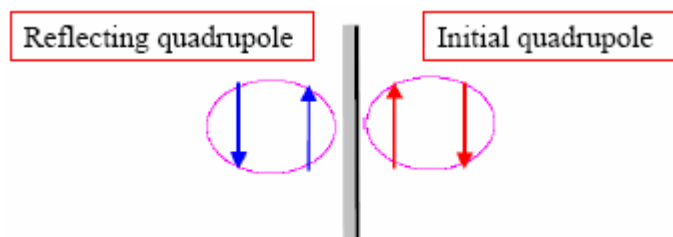


Figure 8. Disappearance of the dipole noise component at the quadrupole reflection from the plane surface.

Hence, if the rear of the element of cylindrical form, operating in the turbulent flow were cut off (flat-end cylinder), the non-compensated dipole component would decrease. Since the cylinder surface curvature variations took place behind the line of the flow separation, the indicated effect was achieved without considerable flow parameter variations and hence, without deterioration of other aerodynamic characteristics. This not evident conclusion is supported by a series of experiments carried out in anechoic chamber, which considers below.

3.4. Analytical confirmation of noise suppression for truncated cylinder

Consider the effects discussed above by careful analytical approach to the 2D problem. For the problem of noise generation by turbulent flow streamlined rigid bodies at small Mach number, near field can be described in terms of incompressible flow, while sound radiated in far field is obtained from the procedure of asymptotical matching with incompressible near field. From this point of view, the multipole expansion of incompressible field determines completely multipole structure of sound radiated.

Let describe incompressible near field in terms of stream function $\psi(\mathbf{r})$ that is expressed through the vorticity $\Omega(\mathbf{r})$ by Poisson equation in the form

$$\Delta\psi(\mathbf{r}) = -\Omega(\mathbf{r}) , \quad (6)$$

where $\mathbf{r} = (x, y)$, under the boundary condition on the rigid surface of the form

$$\psi|_s = const , \quad (7)$$

Note that time dependence will be omitted here, moreover these values can be presented as appropriate Fourier components in some frequency ranges.

For obtaining multipole decomposition of incompressible field at $|\mathbf{r}| \rightarrow \infty$, it is sufficient to consider point vortices $\Omega(\mathbf{r}) = q(\mathbf{r} - \mathbf{r}_0)$ located at point $\mathbf{r}_0 = (x_0, y_0)$. Note that point \mathbf{r}_0 do not have physical sense of coordinates of concrete vortices in turbulent flow, but corresponds to the point of convenient multipole decomposition of wholly vorticity field.

Let $w = w(z)$ is conformal mapping of flow domain to exterior domain of circular cylinder ($|w| \geq a$), then the Green function for this equation corresponds with the case of monopole vortex $q(\mathbf{r} - \mathbf{r}_0) = \delta(\mathbf{r} - \mathbf{r}_0)$ and has the form ²⁷

$$\psi(\mathbf{r}) = -\frac{1}{2\pi} \ln|w(z) - w(z_0)| + \frac{1}{2\pi} \ln \left| w(z) - \frac{a^2}{\overline{w(z_0)}} \right| - \frac{1}{2\pi} \ln|w(z)| , \quad (8)$$

where $z = x + iy$, $z_0 = x_0 + iy_0$, $w = \xi + i\eta$, $\overline{(\cdot)}$ -complex conjugate number.

Two independent quadrupole sources with intensity p correspond to following form of point vortices

$$q_{xx}(\mathbf{r} - \mathbf{r}_0) = p \frac{\partial^2}{\partial x_0^2} \delta(\mathbf{r} - \mathbf{r}_0) ,$$

$$q_{xy}(\mathbf{r} - \mathbf{r}_0) = p \frac{\partial^2}{\partial x_0 \partial y_0} \delta(\mathbf{r} - \mathbf{r}_0) ,$$

so that for determining stream function produced by these sources it is sufficient to differentiate potential (8) with respect to corresponding source position coordinates. It is convenient to represent the exact solution in complex form as follows:

$$\psi_{xx}(\mathbf{r}) = \operatorname{Re} \left\{ \frac{p}{2\pi} \left[\left[\frac{w''(z_0)}{w(z) - w(z_0)} - \frac{1}{w(z) - w^*(\bar{z}_0)} \cdot \frac{2a^2}{(w(\bar{z}_0))^3} \left((w'(\bar{z}_0))^2 - \frac{1}{2} w(\bar{z}_0) w''(\bar{z}_0) \right) \right] + \left(\frac{w'(z_0)}{w(z) - w(z_0)} \right)^2 - \left(\frac{w'(\bar{z}_0)}{w(z) - w^*(\bar{z}_0)} \cdot \frac{a^2}{(w(\bar{z}_0))^2} \right)^2 \right] \right\} \quad (9a)$$

$$\psi_{xy}(\mathbf{r}) = \operatorname{Re} \left\{ \frac{p \cdot i}{2\pi} \left[\left[\frac{w''(z_0)}{w(z) - w(z_0)} + \frac{1}{w(z) - w^*(\bar{z}_0)} \cdot \frac{2a^2}{(w(\bar{z}_0))^3} \left((w'(\bar{z}_0))^2 - \frac{1}{2} w(\bar{z}_0) w''(\bar{z}_0) \right) \right] + \left(\frac{w'(z_0)}{w(z) - w(z_0)} \right)^2 + \left(\frac{w'(\bar{z}_0)}{w(z) - w^*(\bar{z}_0)} \cdot \frac{a^2}{(w(\bar{z}_0))^2} \right)^2 \right] \right\} \quad (9b)$$

where $w^*(\bar{z}_0) = a^2/w(\bar{z}_0)$, $\operatorname{Re}\{ \}$ - the real part of complex number.

To obtain dipole and quadrupole moments, it is necessary to expand expressions (9a,b) at $|z| \rightarrow \infty$ by analogy with (3) in the form

$$\psi = \operatorname{Re} \left\{ \frac{D}{z} + \frac{M}{z^2} + \dots \right\} = \operatorname{Re} \left\{ \frac{D}{z - \zeta} + O\left(\frac{1}{z^3} \right) \right\}. \quad (10)$$

where D and M - dipole and quadrupole moments respectively. At large distance, this field presents as dipole field, however the location of dipole source corresponds with the point $z = \zeta$, for which multipole expansion does not contain quadrupole term. It is easy to obtain the following expression for dipole shift distance

$$\zeta = \frac{M}{D}. \quad (11)$$

First consider the case of circular cylinder of radius a . In this case $w(z) = z$, so that expressions (9a,b) take following form

$$\psi_{xx}(\mathbf{r}) = \operatorname{Re} \left\{ \frac{p}{2\pi} \left(\frac{1}{(z - z_0)^2} - \frac{a^4}{(z - z_0^*)^2 \bar{z}_0^4} - \frac{2a^2}{(z - z_0^*) \bar{z}_0^3} \right) \right\}, \quad (11a)$$

$$\psi_{xy}(\mathbf{r}) = \operatorname{Re} \left\{ \frac{p \cdot i}{2\pi} \left(\frac{1}{(z - z_0)^2} + \frac{a^4}{(z - z_0^*)^2 \bar{z}_0^4} + \frac{2a^2}{(z - z_0^*) \bar{z}_0^3} \right) \right\}, \quad (11b)$$

where $z_0^* = a^2/\bar{z}_0$. In the expressions (11a,b) the first term corresponds with quadrupole field produced by source, the second term corresponds with quadrupole part of the field reflected by cylinder and the third term corresponds with dipole part of the field reflected by cylinder.

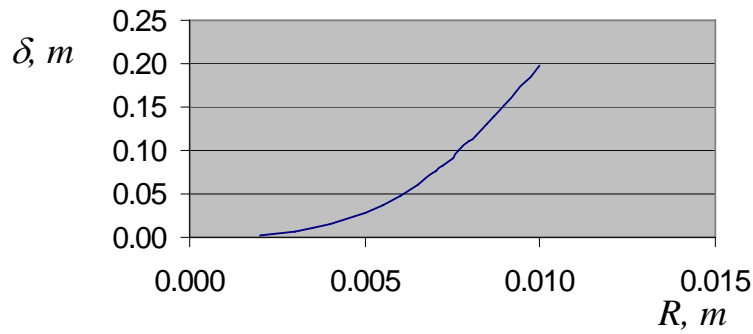


Figure 9. Maximum value of possible shift in incompressible 2D task, as function of distance R between source and cylinder axis (radius of cylinder $a=1.5\text{mm}$).

Thus, the two-dimensional incompressible task shows that the quadrupole sources are closely related to dipole ones and exactly the turbulent fluctuations in the wake near the rod are the direct cause of the dipole noise, which appears to be a reflection of these quadrupole sources. The value of dipole shift in incompressible 2D task, as function of distance R between source and cylinder axis ($z_0 = R$ - position of the point quadrupole source at the axis x) is presented on Figure 9. Since the symmetry of the reflecting obstacle (except the plane) does not correspond to the internal symmetry of quadrupoles, two dipoles forming a quadrupole and cancelling each other “depart” at reflection and are not already completely compensated. This leads to appearing dipole noise in compressible task which repeatedly exceed the reference quadrupole one. However, this initial quadrupole source presence manifests itself as a dipole shift along axis x (3)-(5).

Consider now the effect of cylinder truncation on the dipole moment that is obtained as a result of quadrupole field reflecting from curvature surface. The shape of truncated cylinder with the angle α is presented on Figure 10.

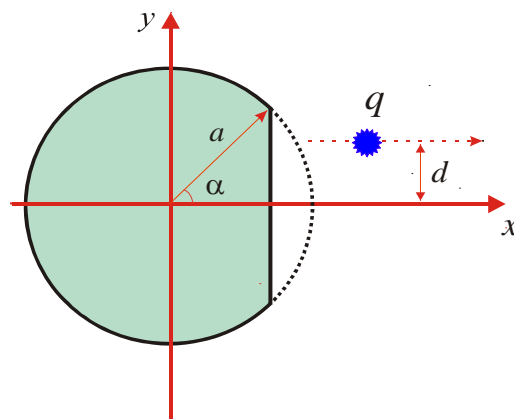


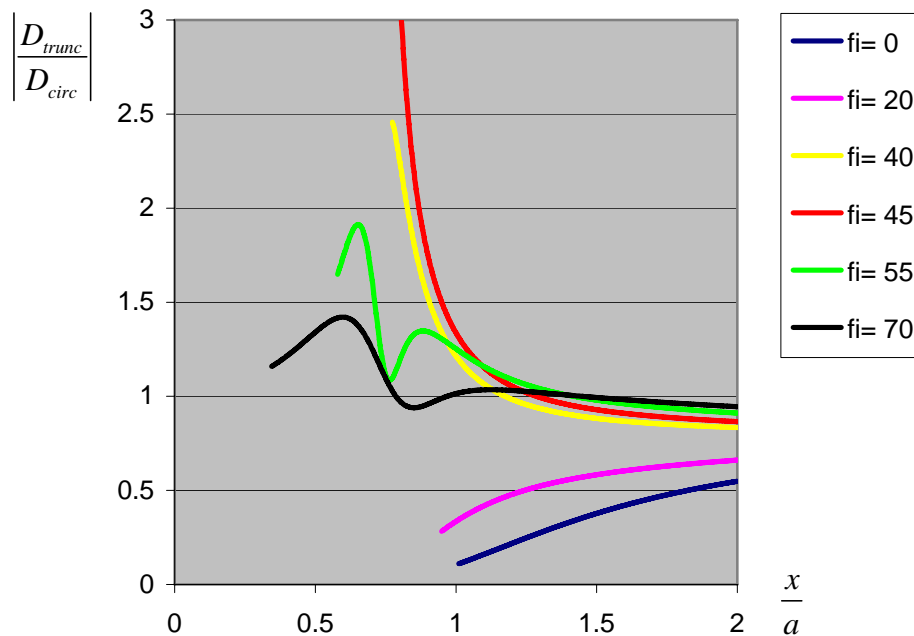
Figure 10. Circular cylinder truncated at the angle α , d - is the distance between x axis and the straight line at which the quadrupole source is located. It is convenient to mark this line through the angle ϕ from the relation $d = a \sin(\phi)$.

In this case the conformal mapping has the following form:

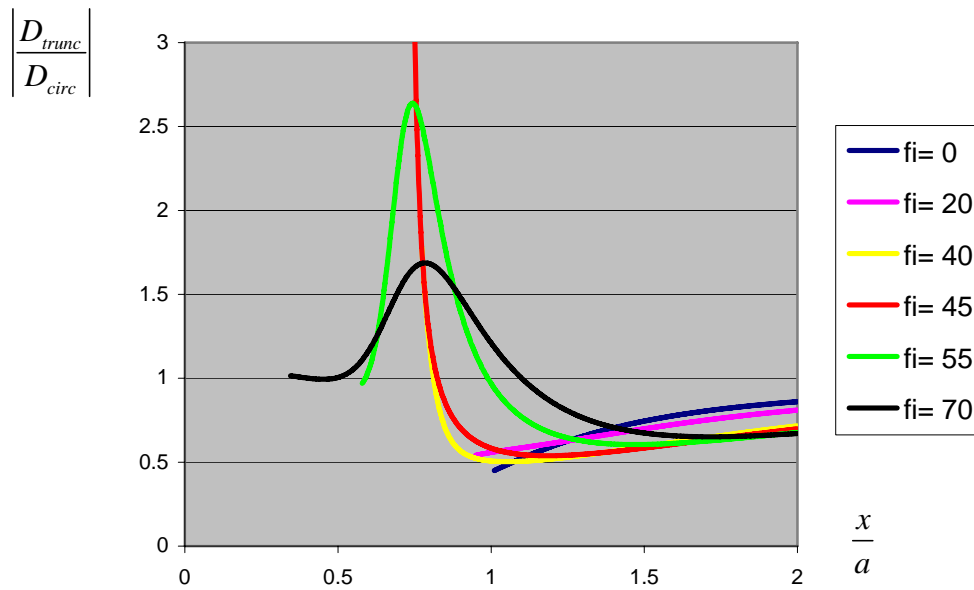
$$w(z) = a \frac{1 - e^{\frac{i\pi^2}{\pi+\alpha}} \left(\frac{a e^{i\alpha} - z}{z - a e^{-i\alpha}} \right)^{\frac{\pi}{\pi+\alpha}}}{\left(\frac{a e^{i\alpha} - z}{z - a e^{-i\alpha}} \right)^{\frac{\pi}{\pi+\alpha}} - e^{\frac{i\pi^2}{\pi+\alpha}}} . \quad (12)$$

Dipole moment created by quadrupole sources situated near truncated cylinder is obtained after substitution (15) into (9a, b) and expanding of the form (10) (it has bulky form and does not given here).

Let quadrupole sources of two kinds are situated along straight line parallel to the x axis at a distance d (it is convenient to mark this line through the angle ϕ from the relation $d = a \sin(\phi)$). Compare the dipole moments induced by quadrupole sources for truncated and circular cylinders. The ratio of induced dipole moment for truncated cylinder with truncated angle $\alpha = 45^\circ$ to one for circular cylinder is presented on Figure 11 for two kinds of quadrupoles as a function of coordinate x along straight lines characterized by different angles ϕ (for each line $x \geq a \cos(\phi)$ that provide the location of the source behind the circular). These calculations show that if quadrupoles sources are situated within zone $-20^\circ \leq \phi \leq 20^\circ$, i.e. in the face of flat-end directly, then induced dipole moments for the case of truncated cylinder decrease essentially as compared with the case of circular cylinder, moreover the closer to flat-end, the more reduction takes place. On the other hand, if quadrupoles sources are situated near the sharp corners of truncated cylinder, then great increasing of induced dipole moment is observed. Thus, this behaviour confirms the qualitative analyse: the induced dipole moments depends directly on the surface curvature near which the quadrupole source is situated. Therefore the dipole moment of flow field which is responsible for both noise radiation and pulsation component of force acting on the cylinder could be increase and decrease depending on source localisation.



a)



b)

Figure 11. Ratio of induced dipole moment for truncated cylinder with truncated angle $\alpha = 45^\circ$ to one for circular cylinder as a function of coordinate x along straight lines characterized by different angles ϕ (for each line $x \geq a \cos(\phi)$ that provide the location of the source behind the circular). (a) q_{xx} - vortex quadrupole source; (b) q_{xy} - vortex quadrupole source.

4. FLAT-END CYLINDER

In this section experimental validation of the main ideas discussed above are presented. The noise generated at lateral turbulent flow past a cylinders in turbulent flow with the velocity of 100 m/s was investigated. Two types of cylinders were examined (Figure 12 a, b): a) with a circular cross-section and b) with a segmented cross-section (flat-end cylinder: a circle with a part cut-off along its chord). The cylinders were placed in the field of developed turbulence of the axisymmetrical jet issuing from the conical nozzle with diameter $D=4$ cm and the initial velocity $V_0 \approx 100 \text{ m/s}$ at the distance of 20 cm from the nozzle exit plane as it was discussed in item 3. The scheme of experimental setup is presented in item 3 too. The generalized measurement results are presented in Figures 13,14.

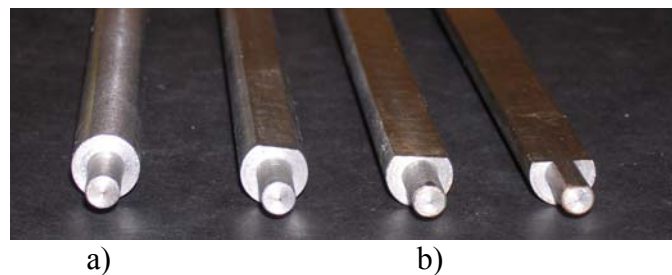


Figure 12. Round and flat-end (truncated) cylinders.

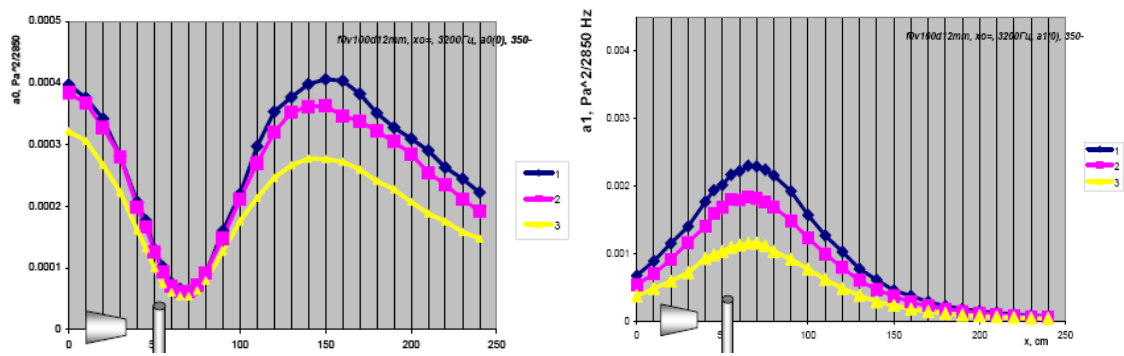


Figure 13. Noise suppression for truncated cylinders, 1 – round cylinder, $D=12$ mm, 2 – small truncation, $L=10.8$ mm, 3 – middle truncation, $L=8.6$ mm, frequency range 350-3200 Hz. a) a_0 , b) a_1 .

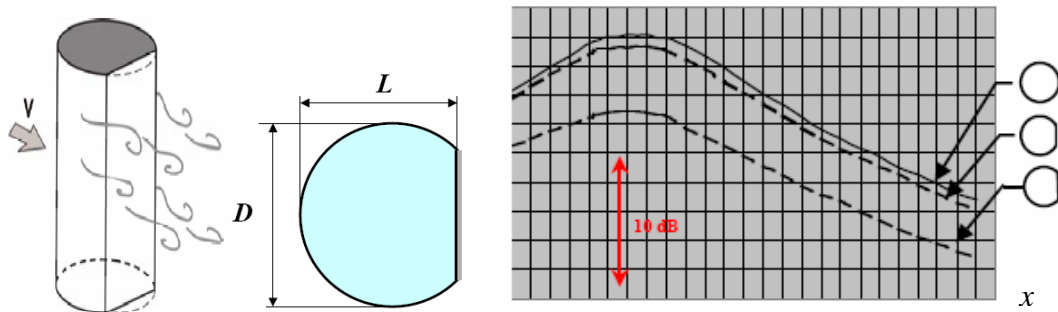


Figure 14. Dependency of the sound pressure level (single microphone) in the frequency bound of 350-3200 Hz on the distance along the jet axis for three types of cylinders $D=12$ mm: a) round cylinder, $L=12$ mm; b) $L=10.8$ mm; c) $L=8.6$ mm

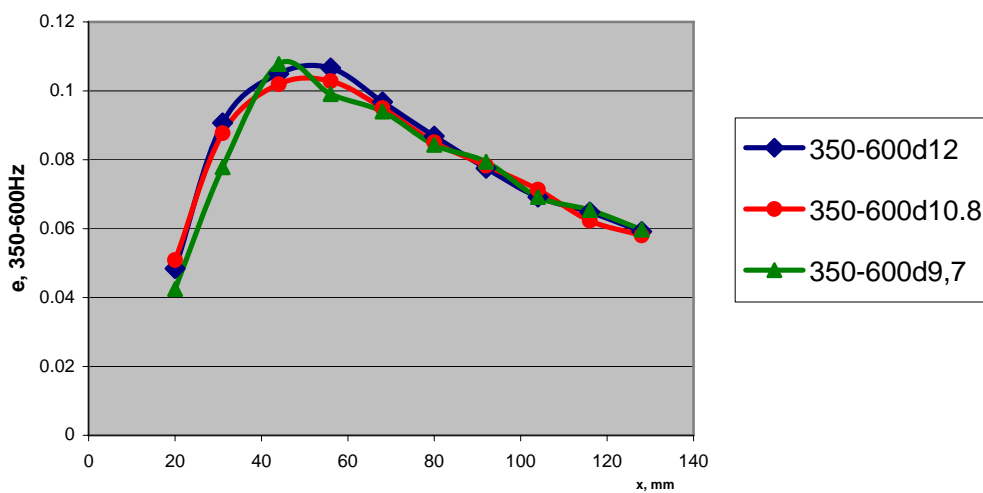


Figure 15. Anemometer measurements of turbulence characteristics behind the cylinder on the axis ($\varepsilon = u'_{rms}(x)/U_0$, U_0 is jet issue velocity 120 m/s). Frequency range 350-600 Hz for three types of cylinders: $D=12$ mm: a) $L=12$ mm; b) $L=10.8$ mm; c) $L=8.6$ mm, which demonstrate identical properties of turbulence behind the round and truncated cylinders.

It was established that for the cylinder with a plane rear surface the noise level in separate frequency bands decreases by the value up to 5 dB over the whole range of observation angles. Note that there are no significant changes in character of turbulence structure in the separation zone for given cylinders compared with circular cylinder. The effect of noise reduction maintained also at a more considerable excision of the cylinder, when the boundaries of the plane part of the cylinder were somewhat ahead of the separation line determined before the excision realization. Therefore the reduction of dipole noise a_0 and a_1 (Figure 13) means that the dipole moment of the flow field is reduced too. It is equivalent to the reduction of pulsating forces in along (draft) and across (lift) flow directions in frequency ranges under consideration.

5. LARGE EDDY SIMULATIONS OF THE FLOW PAST REGULAR AND TRUNCATED CYLINDERS

5.1. Physical model and numerical method

The three-dimensional unsteady Navier-Stokes equations written for a viscous compressible fluid are considered as physical model. Since the direct resolution of these equations for highly turbulent flows should involve a too large range of length and time scales, only the largest scales of the flow are resolved. Any flow variable ϕ is therefore decomposed as $\phi = \bar{\phi} + \phi'$, where $\bar{\phi}$ represents the large scale part of the variable, which is directly resolved, and ϕ' its small scale part that will be modelled. The filtering operator, classically defined as a convolution product on the computational domain, is assumed to commute with time and spatial derivatives. Moreover, it is convenient for the clarity of the equations to introduce the Favre filtering $\tilde{\phi} = \overline{\rho\phi} / \bar{\rho}$. In conservative form, the filtered Navier-Stokes equations are expressed as:

$$\frac{\partial \bar{Q}}{\partial t} + \frac{\partial}{\partial x_i} F_j(\bar{Q}) - \frac{\partial}{\partial x_i} (F_j^v(\bar{Q}) + F_j^{sgs}(\bar{Q})) = 0$$

where $\bar{Q} = (\bar{\rho}, \bar{\rho\tilde{u}}_1, \bar{\rho\tilde{u}}_2, \bar{\rho\tilde{u}}_3, \bar{\rho E})^T$; the convective fluxes F_j , viscous fluxes F_j^v and subgrid terms F_j^{sgs} are respectively defined as:

$$F_j(\bar{Q}) = \begin{pmatrix} \bar{\rho\tilde{u}}_j \\ \bar{\rho\tilde{u}}_1\tilde{u}_j + \delta_{1j}\bar{p} \\ \bar{\rho\tilde{u}}_2\tilde{u}_j + \delta_{2j}\bar{p} \\ \bar{\rho\tilde{u}}_3\tilde{u}_j + \delta_{3j}\bar{p} \\ (\bar{\rho E} + \bar{p})\tilde{u}_j \end{pmatrix} \quad F_j^v(\bar{Q}) = \begin{pmatrix} 0 \\ \sigma_{1j} \\ \sigma_{2j} \\ \sigma_{3j} \\ \sigma_{kj}\tilde{u}_k + q_j \end{pmatrix} \quad F_j^{sgs}(\bar{Q}) = \begin{pmatrix} 0 \\ \tau_{1j} \\ \tau_{2j} \\ \tau_{3j} \\ \tau_{kj}\tilde{u}_k + \varphi_j \end{pmatrix}$$

where the resolved energy is $\bar{\rho E} = \frac{\bar{p}}{\gamma - 1} + \frac{1}{2} \bar{\rho\tilde{u}}_i\tilde{u}_i$.

Classical expressions are used for the viscous stress tensor σ and viscous heat flux vector q , *i.e.*:

$$\sigma_{ij} = 2\mu(\tilde{T}) \left(S_{ij}(\tilde{u}) - \frac{1}{3} \delta_{ij} S_{kk}(\tilde{u}) \right)$$

$$q_j(\tilde{T}) = \frac{\mu(\tilde{T})}{\text{Pr}} \frac{\partial \tilde{T}}{\partial x_j}$$

where T is temperature, Pr the Prandtl number, and $S(\tilde{u})$ is the filtered shear-stress tensor:

$$S_{ij}(\tilde{u}) = \frac{1}{2} \left(\frac{\partial \tilde{u}_i}{\partial x_j} + \frac{\partial \tilde{u}_j}{\partial x_i} \right)$$

Sutherland's law is used to compute the viscosity μ as a non-linear function of the temperature. These equations are supplemented with the filtered perfect gas state law.

The parameterizations of the subgrid stress tensor τ and subgrid heat flux vector φ (assuming usual approximations³² and using Boussinesq eddy viscosity hypothesis) are:

$$\tau_{ij} = 2\mu_{sgs} \left(S_{ij}(\tilde{u}) - \frac{1}{3} \delta_{ij} S_{kk}(\tilde{u}) \right)$$

$$\varphi_j = \frac{\mu_{sgs}}{\text{Pr}_t} \frac{\partial \tilde{T}}{\partial x_j}$$

The selective mixed scale model, developed by Sagaut and Lenormand^{33, 34, 35}, has been retained as subgrid closure. The additional use of a selective function allows handling of transitional flows.

The eddy viscosity is given by the non-linear combination:

$$\mu_{sgs} = \bar{\rho} f_s(\theta) C_m \Delta^{3/2} (2S_{ij}(\tilde{u})S_{ij}(\tilde{u}))^{1/4} q_{sgs}^{1/4}$$

of the filtered shear stress tensor $S_{ij}(\tilde{u})$, the cut-off length scale Δ (cube root of the cell volume in the present study), the small scale kinetic energy $q_{sgs} = (u'_i u'_i) / 2$, a modelling parameter $C_m = 0.06$ and the following selective function:

$$f_s(\theta) = \begin{cases} 1 & \text{if } \theta > \theta_0 = 10^\circ \\ \frac{\tan^4(\theta/2)}{\tan^4(\theta_0/2)} & \text{if } \theta \leq \theta_0 \end{cases}$$

where θ denotes the angle between the instantaneous and filtered vorticity vectors. The test field u'_i is approximated from the resolved field $u'_i \approx \tilde{u}_i - \hat{u}_i$, employing a discrete averaging test filter derived from the following mono-dimensional approximation:

$$\hat{\phi}(x_i) = \frac{1}{4} \tilde{\phi}(x_{i-1}) + \frac{1}{2} \tilde{\phi}(x_i) + \frac{1}{4} \tilde{\phi}(x_{i+1})$$

The set of the unsteady filtered Navier-Stokes equations is solved using a structured multi-block solver, developed at ONERA for aeroacoustic studies^{28, 29, 30, 31}. The present simulations have been carried out using a modified version³⁶ of the

AUSM+P finite volume scheme to discretize the convective fluxes. This scheme takes advantage of a wiggle detector that allows limiting of the numerical dissipation where odd-even wiggles are detected. With this modification, the numerical scheme essentially acts as a second order centered scheme which is well suited for LES, while remaining stable for realistic configurations. For full details, see the paper by Mary and Sagaut³⁶. The viscous fluxes are discretized using a second-order accurate centered formula. Finally, time advancement is performed using a third order accurate explicit Runge-Kutta scheme with a maximum CFL number of 0.95.

5.2. Computational setup

Two configurations have been simulated using LES: a first one consisting of the flow around a regular circular cylinder, and a second one in which the cylinder is truncated in its rear part, with a truncation angle of $\pm 45^\circ$ with respect to the x -axis (see Figure 16).

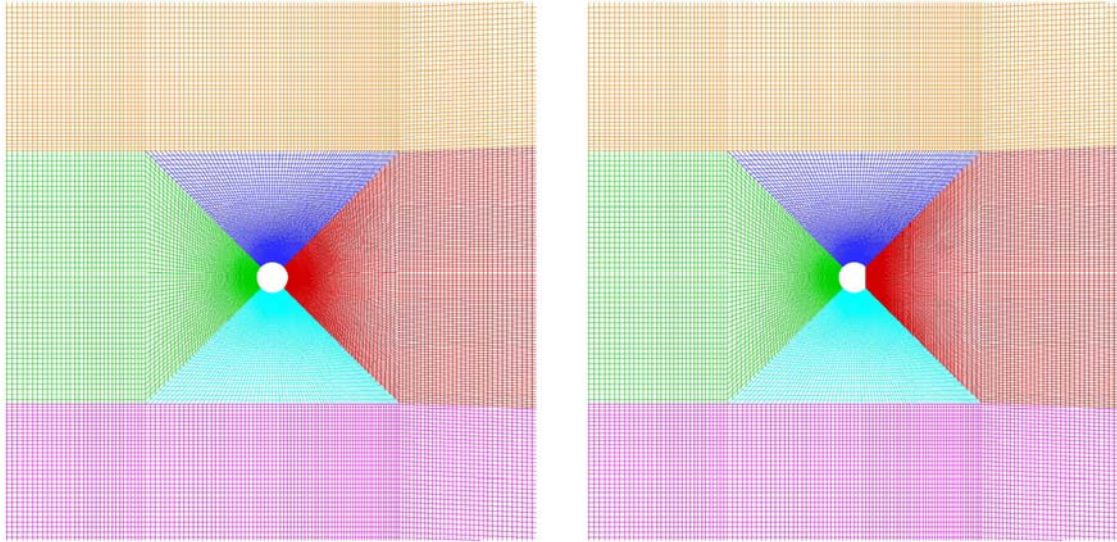


Figure 16. Close view of the mesh near the cylinder. Left: regular cylinder geometry. Right: truncated cylinder geometry.

In both cases, the incoming flow has a uniform speed $U_\infty = 70m/s$, and the diameter of the cylinder d is set to $3mm$. The associated Reynolds number is $Re=15,000$, therefore yielding to a fully turbulent flow around the cylinder and in its wake. These parameters differ from the experimental ones, and have been adjusted to keep a reasonable value of the Reynolds number, and avoid the use of too huge grids while resolving correctly the flow. For this reason, only qualitative comparisons with the experimental observations will be performed in this study.

Three-dimensional computational grids have been considered. The computational domain extends to $200d$ away from the cylinder axis in the streamwise (x) and vertical (y) directions, the grid resolution making it possible to resolve correctly the acoustic waves associated to the fundamental vortex shedding frequency up to $100d$ away from the cylinder. The spanwise extent of the computational domain is $L_z=3d$, which is sufficient to account for three dimensional effects in the wake. To save computational resources a 2D/3D coupling strategy is used: the grid is only three-dimensional in the central area surrounding the cylinder and its wake - where the flow is expected to be fully turbulent and 3D - and two-dimensional in the upper and lower parts, where only 2D acoustic waves are present. In the 3D part, 32 grid points are used

in the spanwise direction. A radial stretching of the mesh is used, such that the smallest cell at the cylinder surface corresponds to a radial step of $5 \cdot 10^{-3}d$, while ensuring a proper resolution of the acoustic waves up to $100d$. The azimuthal discretization uses 290 grid points, with also grid stretching applied such that the discretization in the rear part of the cylinder is finer than in the front one where the flow remains essentially laminar. For both calculations, the overall number of points used is slightly larger than 2 millions. Figure 16 displays a close view of the mesh near the cylinder. It can be observed that this mesh is decomposed into six different blocks.

5.3. Acoustic results comparison

The first objective of these simulations is to check if the noise reduction property of the truncated geometry can be - at least qualitatively - reproduced by numerical simulation. All the results presented below are extracted after a sufficient transient time after which a statistical steady state of the flow is reached.

Figure 17 displays 2D snapshots of isocontours of the dilatation field $\theta = \nabla \cdot u$, which makes it possible to highlight the circular acoustic waves emitted at the cylinder. The first observation is that the main sound source seems to act as a dipole. The same levels are considered on the left and right sides of the figure. It therefore clearly appears here that the acoustic waves emitted from the cylinder have a significantly larger amplitude with the baseline cylinder geometry than with the truncated one.

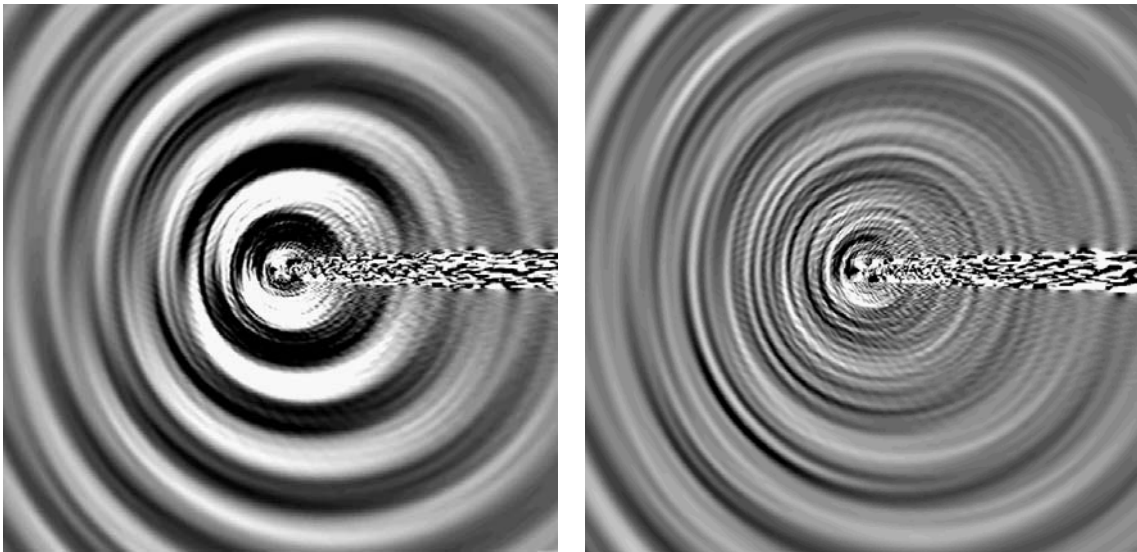


Figure 17. Acoustic waves visualization (dilatation field). Left: regular cylinder geometry. Right: truncated cylinder geometry.

This can be checked by looking at directivity diagrams of the *rms* pressure, displayed in figure 18, at respectively 10 and 100 diameters away from the cylinder. Notice that in these plots, the reference pressure to compute the levels in decibels has been taken as $p_{ref} = 1 Pa$ instead of the usual value $p_{ref} = 2 \times 10^{-5} Pa$, in order to highlight the differences between the two geometries. There, it is clear that the radiated acoustic levels for the truncated geometry are decreased by about 2 dB in each direction in comparison with the regular one. This is also clear when looking at figure 19, displaying the streamwise evolution of the *rms* pressure level, at a height of 70

diameters above the x axis (as it was done in the experiments). Here, it can be observed that there is an excellent qualitative agreement with the experimental observations (see Figure 14), with a reduction of about 2 dB of the acoustic levels.

Figure 20 presents pressure spectra computed respectively at the surface of the cylinder and at 4 diameters away from its axis. It can be seen that the main peak is observed at a Strouhal number of about 0.18. At this frequency, it appears that the truncated cylinder configuration leads to a lower peak, by about 5 dB.

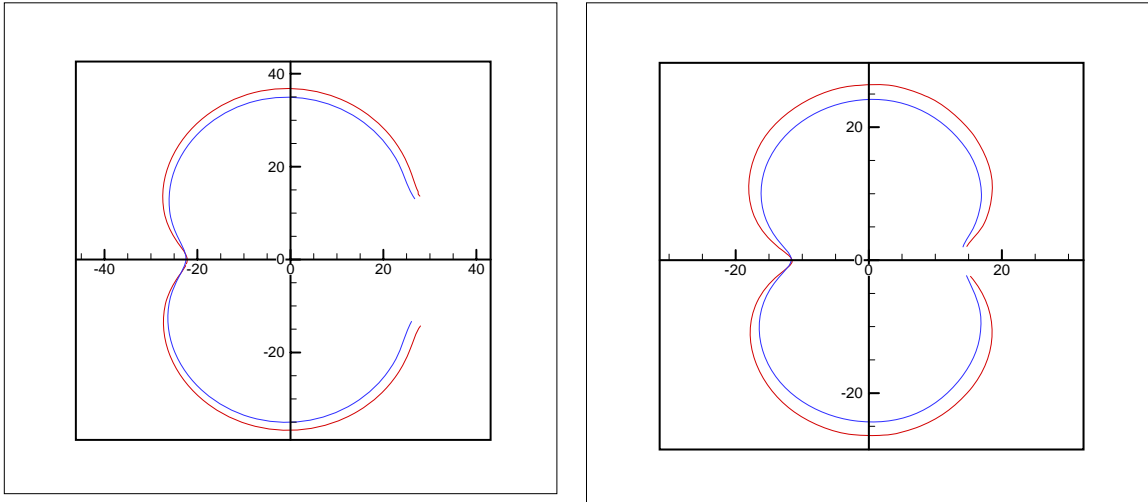


Figure 18. Directivity diagrams in dB , computed at $r=10d$ (left) and $r=100d$ (right) away from the cylinder's axis. Note that the reference pressure is taken as $1 Pa$ instead of $2 \cdot 10^{-5} Pa$ to highlight the differences between the two configurations. Red line: baseline configuration. Blue line: truncated cylinder

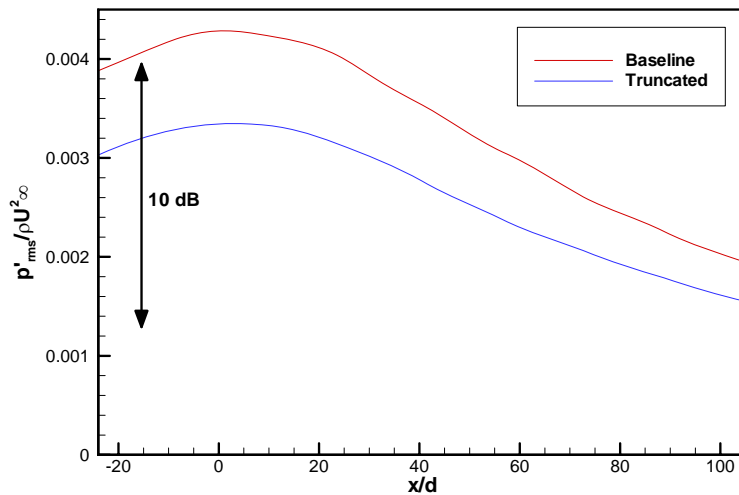


Figure 19. Dependency of the computed sound pressure level (at $y=70d$) on the distance along the jet axis.

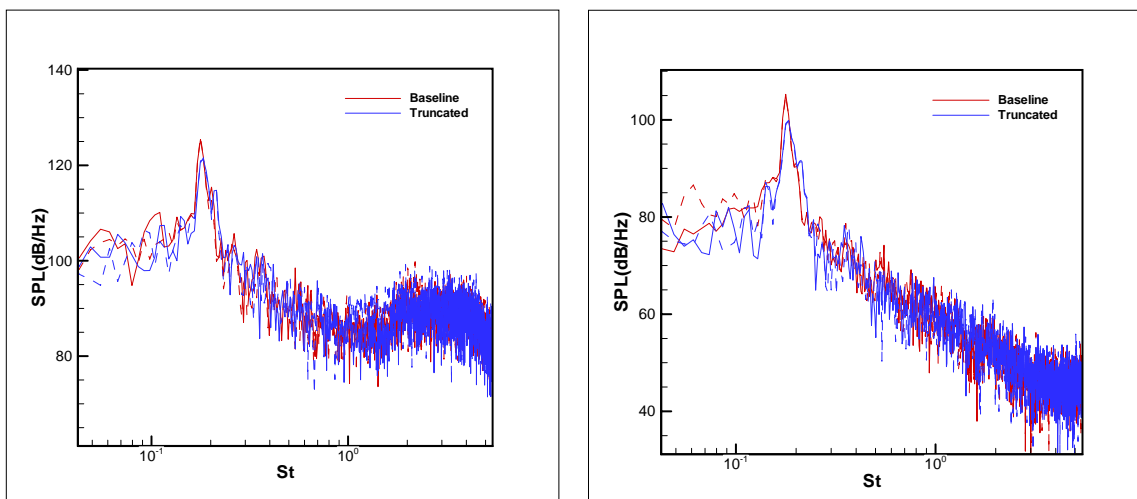


Figure 20. Pressure spectra computed in the upper (solid lines) and lower (dashed lines) parts of the domain. Left: points located at the surface of the cylinder ($\pm 90^\circ$ with respect to the x -axis). Right: points located at $y = \pm 4d$.

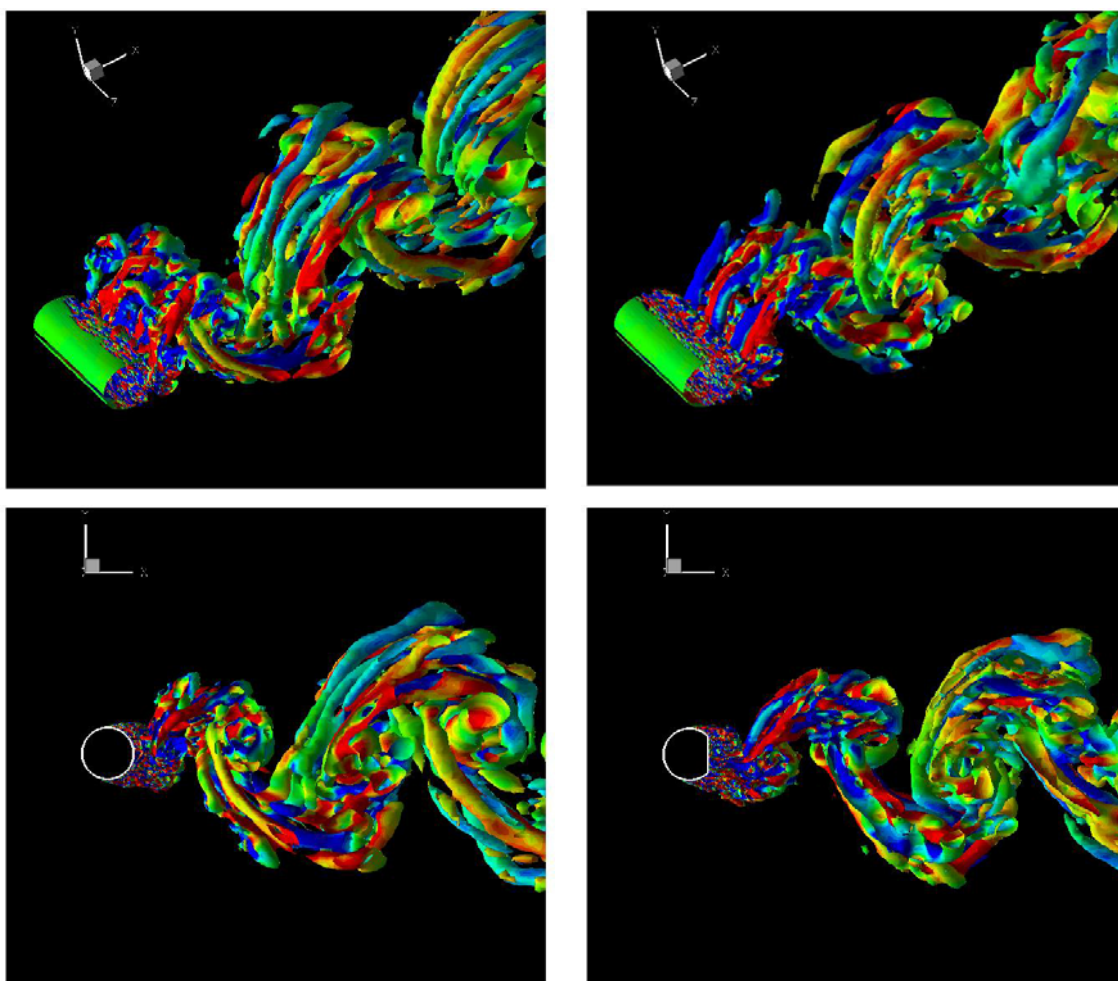


Figure 21. Three-dimensional view of the flow (iso-Q surface coloured by the streamwise component of vorticity). Left: regular cylinder geometry. Right: truncated cylinder geometry.

5.4. Aerodynamic results comparison

In the previous section, it has been observed that the truncated geometry leads to lower noise levels, as it was expected theoretically and was also observed in the experiments. The aim of this section is to investigate how the flow itself is modified by considering the truncated cylinder, and see if some specific aerodynamic features may be responsible for the noise reduction effect.

Unsteady flow features

Figure 21 presents three dimensional visualizations of the flow for each cylinder geometry. This is made possible by extracting iso-surfaces of the Q criterium defined as:

$$Q = \frac{1}{2} (S_{ij} S_{ij} - \Omega_{ij} \Omega_{ij})$$

$$\text{where } S_{ij} = \frac{1}{2} \left(\frac{\partial \tilde{u}_i}{\partial x_j} + \frac{\partial \tilde{u}_j}{\partial x_i} \right) \text{ and } \Omega_{ij} = \frac{1}{2} \left(\frac{\partial \tilde{u}_i}{\partial x_j} - \frac{\partial \tilde{u}_j}{\partial x_i} \right).$$

This quantity makes it possible to investigate the coherent turbulent structures present in the flow. It is observed that for both cases, 2D spanwise structure occur at large scale, forming the well-known Karman vortex street behind the cylinder. Between them, 3D contra-rotative elongated filaments, usually referred to as "ribs", are observed, and fine scale turbulence occurs near the cylinder surface. From these views there only seems to be a small decrease in the turbulence level for the truncated geometry, but no striking difference between the two configurations can really be observed at this point.

Figure 22 displays a numerical Schlieren view (density gradient magnitude) close to the cylinder surface. It can be seen that there is a high level of fine-scale turbulence in the recirculation area behind the cylinder in both case. However, it can be observed that the large-scale oscillation of the wake for the baseline geometry appears much stronger than with the truncated geometry. This stabilization effect of the truncation is clearly confirmed by looking at some movies of the flow. As a consequence, the fluctuation of the aerodynamic force acting on the cylinder is lower in this case. It can therefore be thought that this feature of the truncated geometry may be responsible for a reduction in the noise generation process at the cylinder's upper and lower surfaces.

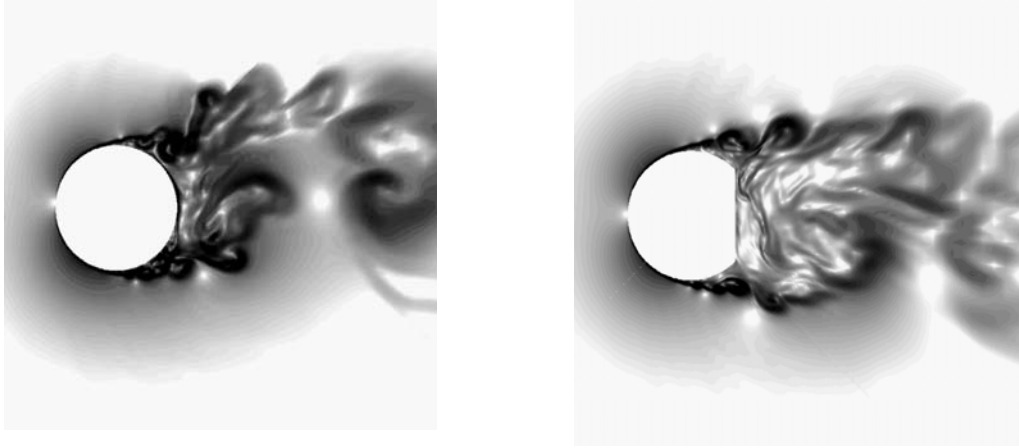


Figure 22. Numerical Schlieren view of the turbulent flow near the cylinder. Left: regular cylinder geometry. Right: truncated cylinder geometry.

Mean flow features and turbulence statistics

Figure 23 presents the mean flow streamlines computed in each case. It can be seen that the mean recirculation area behind the cylinder extends to the same location behind the cylinder with and without truncation, and that the mean flow is only modified in the vicinity of the cylinder. For both cases, mean separation occurs at the same location.

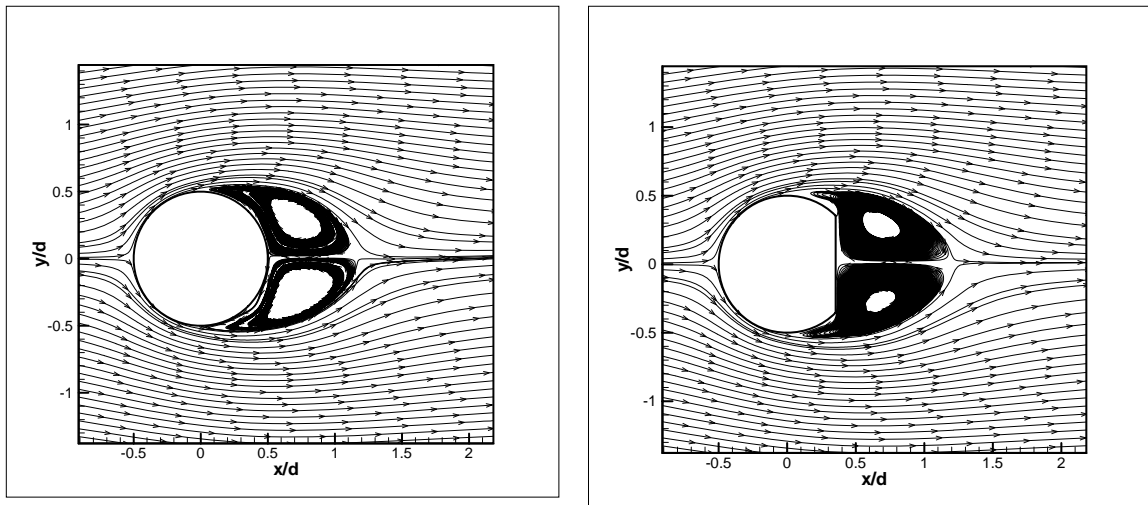


Figure 23. Mean flow streamlines. Left: regular cylinder geometry. Right: truncated cylinder geometry.

Figure 24 displays the resolved turbulent kinetic energy $k_{rms} = \frac{1}{2} u'_{i,rms}$ in the vicinity of the cylinder. Higher levels are observed for the regular cylinder geometry, indicating that the truncation of the cylinder also tends to decrease the turbulence intensity in the recirculation area behind the cylinder. Figure 25 makes it possible to compare streamwise variation of turbulence characteristics along the x -axis behind the cylinder with the experimental ones (see Figure 15). It appears that the peak value is significantly higher than in the experiment, and occurs at a location which is closer from the cylinder. A possible explanation is that the experimental results only account for the frequency range 350-600 Hz, and therefore neglect the contribution of small, non-radiating but energetic, turbulent scales. Again, it can be seen that the global level of the turbulent fluctuations is reduced for the truncated cylinder. However, the global

behavior remains the same, indicating that the flow characteristics are not strongly modified.

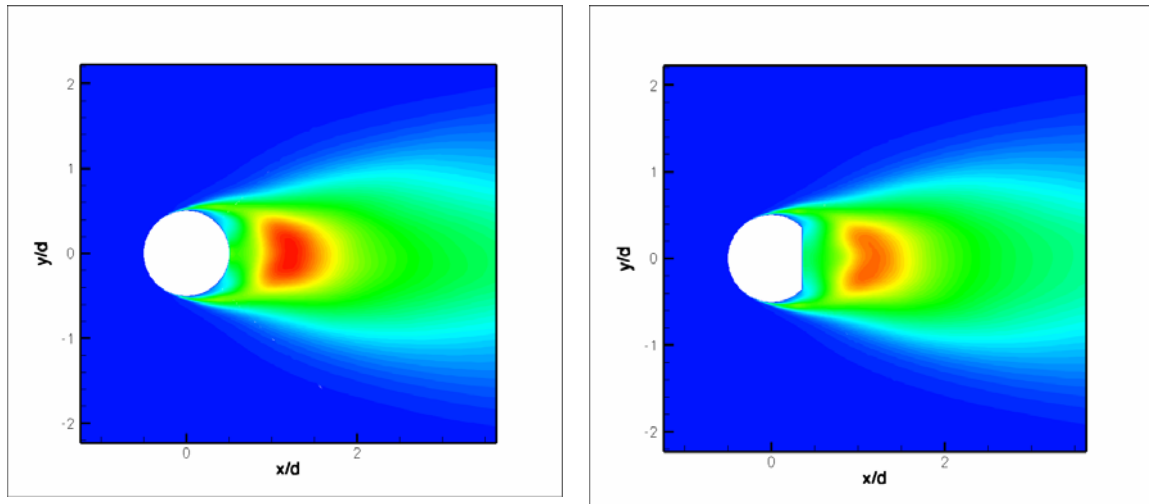


Figure 24. Iso-value map of resolved turbulent kinetic energy. Levels ranging from $k_{rms} = 0$ (blue) to $k_{rms} = 0.5 U_{\infty}^2$ (red).

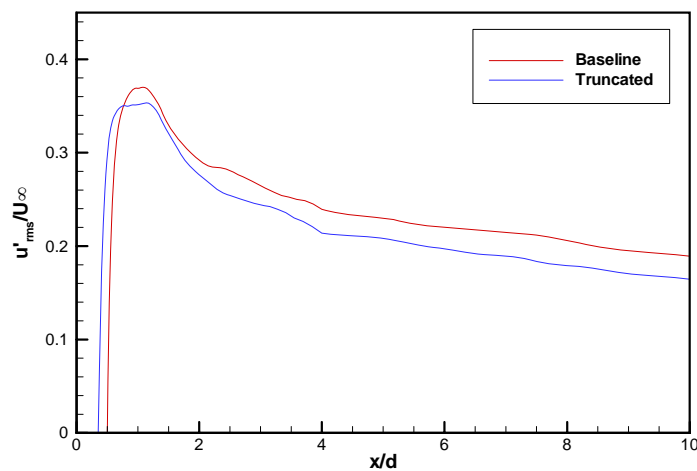


Figure 25. Streamwise evolution of the rms streamwise velocity fluctuation behind the cylinder.

6. CONCLUSIONS

Abnormal radiation directivity is revealed which corresponds to the effective dipole displacement into the wake region for a distance of ~ 10 cylinder diameters. It is shown that the effect of the dipole shift is connected with the interference of two sources: quadrupoles in the separation zone and the reflected dipoles induced by them. The reflected dipoles are shown to be generated due to the curvature of reflection surface and their sound pressure level exceeds many times the quadrupoles in the far field.

Exact solution of model problem on quadrupole near the round cylinder and truncated cylinder for 2D cases are obtained, dipole shift is revealed and maximum value of achievable shift in compressible task as a function of quadrupole location is found. The understanding of the effect of dipole abnormal shift as self-tuning effect for reflected quadrupole helps to elaborate the modified cylinder configurations, which lead to considerable noise suppression. Experimental results for flat-end cylinders were discussed. It was established that for the cylinder (nose leg or engine stator rack) with a plane rear surface the noise level in wide frequency band decreases by the value up to 5 dB over the whole range of observation angles. These configurations present attractive variant of noise control where it is realized by self-tuning of reflected signal leading to suppression of uncompensated dipoles.

Careful 3D numerical simulation of dipole noise for the cylinders (round and truncated) using LES was carried out. Numerical calculation is firstly validated by measurements under consideration. Numerical results are in agreement with the main conclusion that truncation of cylinder leads to noise suppression in wide frequency range. Therefore streamlining the cylinder could be considered as a new benchmark problem in airframe noise field. This problem demonstrates the measure of our success in describing of main peculiarities of novel experiments.

ACKNOWLEDGEMENTS

The work is partly realized with the support of Russian Foundation of Basic Research (05-01-00670) and INTAS (04-80-7043).

REFERENCES

- [1] W. Dobrzynski, L.C. Chow, P. Guion, D. Shiells, "Research into Landing Gear Airframe Noise reduction", AIAA Paper N2002-2409.
- [2] Curle N. The Influence of Solid Boundaries on Aerodynamic Sound. Proc. Roy. Soc. (London) Ser.A. 231, 1187,505-514, 1955
- [3] Goldstein M.E. Aeroacoustics. McGrawHill, 1976.
- [4] Phillips O.M. The Intensity of Aeolian Tones, J.Fluid Mech., 1, pt.6, 607-624, 1956
- [5] Powell A. Aerodynamic Noise and the Plane Boundary. J. Acoust. Soc. Am., 32,8,982-990, 1960. Ser.A, 254, 129-145, 1960.
- [6] Doak P.E. Acoustic Radiation from a Turbulent Fluid Containing Foreign Bodies. Proc. Roy Soc. (London), 31.
- [7] Ffowcs Williams J.E. 'Noise Source Mechanisms' in Modern Methods in Analytical Acoustics: lecture notes, edited by D.G. Crighton, Springer-Verlag London Limited, 1992, pp. 313-354.
- [8] Meecham W.C. 'Surface and volume sound from boundary layers' Journal of the Acoustical Society of America, 1965, v. 37, pp. 516-522.
- [9] Rienstra S.W. and Hirschberg A. 'An Introduction to Acoustics' Eindhoven University of Technology, 2001, 345 pp.

- [10] Davies H.G. ‘The Radiated Fields of Multipole Point Sources Near a Solid Spherical Surface’, *J. Fluid Mech.*, 1970, v.43, pp. 597-606.
- [11] Iida A., Mizuno A. Kato C. ‘Visualization of aerodynamic sound source with compact Green function’, *AIAA paper 2002-2572* (2002)
- [12] Yahathugoda I.D., Akishita S. ‘Simulation on effect of surface impedance for reducing aerodynamic sound from circular cylinder’, *AIAA 2002-2434* (2002)
- [13] V.F. Kopiev, M.Yu. Zaitsev, R.K. Karavosov “Experimental Investigation of Azimuthal Structure of Dipole Noise for Rigid Cylinder Inserted in Turbulent Jets”, *AIAA Paper 2004-2927*.
- [14] Kopiev V.F., M.Yu. Zaitsev, N.N. Ostrikov “New noise source mechanism of flow/surface interaction as applied to airframe noise reduction” *AIAA Paper 2006-2717*
- [15] Kopiev V.F., Zaitsev M. Yu., Chernyshev S.A. Sound radiation from a free vortex ring and a ring crossing an obstacle. *AIAA Paper 98-2371*, 1998, 14 p.
- [16] Zaitsev My, Kopiev VF and Kotova AN (2001) On Decomposition of turbulent vortex ring noise into elementary quadrupoles. *Acoust Phys* 47, 699-706 (translated from *Acoust Zurn* 47, 793-801).
- [17] Kopiev V. F., Zaitsev M. Yu., Chernyshev S.A. and Kotova A. N. The Role of Large-Scale Vortex in a Turbulent Jet Noise. *AIAA paper 99-1839*, 1999, 13 p.
- [18] V.F. Kopiev, M.Yu. Zaitsev, R.K. Karavosov. On azimuthal structure of supersonic jet noise. *Proceedings of Tenth International Congress of Sound and Vibration ICSV10, Stockholm, Sweden, 2003, v.2, p.637-644*
- [19] Kopiev VF (2004) Azimuthal decomposition of turbulent jet noise and its role for diagnostics of noise sources. *VKI Lecture Series 2003-04 "Advances in Aeroacoustics and Applications"*.
- [20] Crow SC ‘Aerodynamic sound emission as a singular perturbation problem’ *Stud. Appl. Math.* 1970, v.49, N1,21-44
- [21] Kopiev V.F. Chernyshev S.A. ‘Mach-number expansion of the sound field produced by localized vortices, *Acoust. Phys.* v.41, 546-551.
- [22] Landau L D, Lifshitz E M *Teoreticheskaya Fizika Vol. 2 Theory of field*, Moscow: Nauka, 1986) [Translated into English (London: Pergamon Press, 1987)]
- [23] Howe M. *Theory of vortex sound*, Cambridge, 2003
- [24] Felsen L.B., Marcuvitz N. *Radiation and scattering of waves*, v.2, Prentice-Hall, Inc., Englewood Cliffs, New Jersey, 1973
- [25] Dobrzynski, W., Buchholz, H., “Full-Scale Noise Testing on Airbus Landing Gears in the German Dutch Wind Tunnel”, *AIAA/CEAS Meeting Paper 97-1597*, 3rd AIAA/CEAS Aeroacoustics Conference, Atlanta/USA, May 12-14, 1997.
- [26] Dobrzynski, W., Schoning B., Leung C., Wood C., Smith M., Seror Ch. Design and Testing of Low Noise Landing Gears *AIAA/CEAS Paper 2005-3008*
- [27] Milne-Tomson L.M. *Theoretical Hydrodynamics*, MacMillan, NY, 1960

- [28] Terracol M., Manoha E., Herrero C., Labourasse E., Redonnet S. and Sagaut P. “Hybrid methods for airframe noise numerical prediction”, *Theoretical and Computational Fluid Dynamics*, 19: 197-227, 2005.
- [29] Desquesnes G., Terracol M., Manoha E. and Sagaut P. “On the use of a high order overlapping grid method for coupling in CFD/CAA”, *J. Comput. Phys.*, 220(1): 355-382, 2006.
- [30] Terracol M., “A Zonal RANS/LES Approach for Noise Sources Prediction”, *Flow, Turbulence Combust.*, 77: 161-184, 2006.
- [31] Desquesnes G., Terracol M. and Sagaut P. “Numerical investigation of the tone noise mechanism over laminar airfoils”, *J. Fluid. Mech.*, in press, 2007.
- [32] Vreman B., Geurts B. and Kuerten H. “A priori tests of large eddy simulation of the compressible plane mixing layer”, *J. Engineering Math*, 29(4): 299-327, 1995.
- [33] Sagaut P. “Large Eddy Simulations of incompressible flows. An introduction”, third edition, Springer-Verlag, 2005.
- [34] Lenormand E., Sagaut P. and Ta Phuoc L. “Large Eddy Simulations of Subsonic and Supersonic Channel Flow at Moderate Reynolds Number”, *Int. J. Numer. Meth. Fluids*, Vol. 32, pp. 369-406, 2000.
- [35] Lenormand E., Sagaut P., Ta Phuoc L. and Comte P. “Subgrid-Scale Models for Large Eddy Simulations of Compressible Wall Bounded Flows”, *AIAA Journal*, Vol. 38, pp. 1340-1350, 2000.
- [36] Mary I. and Sagaut P. “Large Eddy Simulation of Flow Around an Airfoil Near Stall”, *AIAA J.*, 40(6): 1139-1145.